# Surface atomic relaxation and magnetism on hydrogen-adsorbed Fe(110) surfaces from first principles

Urslaan K. Chohan[a,b], Enrique Jimenez-Melero[a,b], Sven P.K. Koehler[b,c,d,*]

[a]*School of Materials, The University of Manchester, Manchester M13 9PL, UK*
[b]*Dalton Cumbrian Facility, The University of Manchester, Moor Row CA24 3HA, UK*
[c]*School of Chemistry, The University of Manchester, Manchester M13 9PL, UK*
[d]*Photon Science Institute, The University of Manchester, Manchester M13 9PL, UK*

## Abstract

We have computed adsorption energies, vibrational frequencies, surface relaxation and buckling for hydrogen adsorbed on a body-centred-cubic Fe(110) surface as a function of the degree of H coverage. This adsorption system is important in a variety of technological processes such as the hydrogen embrittlement in ferritic steels, which motivated this work, and the Haber-Bosch process. We employed spin-polarised density functional theory to optimise geometries of a six-layer Fe slab, followed by frozen mode finite displacement phonon calculations to compute Fe-H vibrational frequencies. We have found that the quasi-threefold (3f) site is the most stable adsorption site, with adsorption energies of $\sim 3.0\,\mathrm{eV/H}$ for all coverages studied. The long-bridge (lb) site, which is close in energy to the 3f site, is actually a transition state leading to the stable 3f site. The calculated harmonic vibrational frequencies collectively span from 730 to $1220\,\mathrm{cm^{-1}}$, for a range of coverages. The increased first-to-second layer spacing in the presence of adsorbed hydrogen, and the pronounced buckling observed in the Fe surface layer, may facilitate the diffusion of hydrogen atoms into the bulk, and therefore impact the early stages of hydrogen embrittlement in steels.

*Keywords:* ferritic steels, hydrogen embrittlement, Density Functional Theory, adsorption, Haber–Bosch process

*[*]Corresponding author*:
University of Manchester
School of Chemistry
Oxford Road
Manchester
M13 9PL
United Kingdom.
Tel.: +44 161 306 4448
Email: sven.koehler@manchester.ac.uk

## 1. Introduction

Key structural materials are exposed to a continuous supply of hydrogen in a wide range of technological applications, ranging from hydrogen containment in hydrogen-energy [1] and petrochemical applications [2] to hydrogen continuously produced from water radiolysis in nuclear power plant and waste storage applications [3]. Hydrogen presents limited solubility in most metallic materials [4], and can potentially induce enhanced fatigue and premature fracture [5]. The current understanding of the hydrogen-induced embrittlement and failure mechanisms is mainly based on the interaction of hydrogen atoms with localised plasticity [6]. This interaction can result in enhanced crack propagation rates and premature failure [7]. The ultimate goal is to predict the resistance of a given structural material to environmental hydrogen attacks, based on its current damage state and the predicted service conditions. In order to produce reliable predictions of materials' performance in hydrogen-rich environments, an overarching theory and proper modelling tools should be developed and tested in terms of the hydrogen intake, its diffusion through the defect structure of the bulk material, and its interaction with the local lattice defects and plasticity in the vicinity of hydrogen-trapping sites. The first stepping stone in this global process is the gaseous hydrogen-metal interaction that leads to hydrogen adsorption and subsequent intake by the bulk metal.

We have focused this work on Fe-based systems due to the increasing importance of ferritic steels and their hydrogen-enhanced degradation modes in gas pipeline [8, 9] and next generation reactor applications [10, 11]. Iron crystallises in a body-centred cubic (bcc) structure, namely ferrite phase, at temperatures below 912 °C [12]. Ferritic steels develop characteristic grain orientation distributions during thermo-mechanical processing, where a significant number of grains in the polycrystalline material present their (110) crystal planes parallel to the surface of the material [13]. Therefore, the interaction between hydrogen and Fe(110), and subsequent hydrogen adsorption on the surface constitute the first steps in the mechanism of hydrogen embrittlement in ferritic steels and, consequently, also the first opportunity in delaying or preventing the premature failure of these materials operating in hydrogen-rich environments. While this work was motivated by and focussed on hydrogen embrittlement in steels, it is worth mentioning that adsorption of hydrogen on iron is also the first step in the Haber-Bosch process converting $H_2$ and $N_2$ gas into ammonia, most notably used as a feedstock for fertiliser production [14].

The interaction of gaseous $H_2$ molecules with the metallic surface is believed to start with the process of physisorption enabled by weak van der Waal forces. The binding energy

of the $H_2$ molecules to the surface is ~0.04-0.15 eV/$H_2$ [15]. The mobile physisorbed hydrogen molecules may then migrate to active dissociation centres on the surface, where they will dissociate to form atomic hydrogen [16]. The chemisorbed H atoms would then diffuse parallel to the metallic surface until they become trapped at specific adsorption sites [15]. The heat of adsorption is reported to be ~1.1 eV/$H_2$ [16, 17]. Fig. 1 shows potential adsorption sites for H atoms on the Fe(110) surface: on-top of an iron atom from the top surface layer (ot site), in between two Fe atoms either in a short or long-bridge position (two-fold sb and lb sites, respectively), or surrounded by three surface Fe atoms arranged in an isosceles triangle (quasi-threefold 3f site). The preferred site(s) for the H-atoms to reside depends on both the potential energy landscape at the surface and the repulsive interaction between adsorbed hydrogen. We can define the degree of coverage $\theta_H$ as the ratio between the number of adsorbed H-atoms and iron atoms.

Unfortunately, some physical properties of the hydrogen adsorption process on Fe surfaces are still not known with certainty, such as the vibrational frequencies of the adsorbate-substrate, as well as the binding energies and lattice relaxation as a function of hydrogen coverage. The amount of experiment work on the H-Fe(110) system up to date is limited, mainly due to the difficulties related to the preparation of clean oxide-free Fe(110) single crystal surfaces under ultra-high vacuum. The results derived from Low Energy Electron Diffraction (LEED) experiments led to the identification the $(2 \times 1)$, $(3 \times 1)$, and $(1 \times 1)$ motifs of H adsorbed on the Fe(110) surface for coverages of 50, 67, and 100 %, respectively [16, 18, 19]. Additionally, a graphitic $(2 \times 2)$-2H phase has been found experimentally at temperatures below $-193\,°C$ [20]. However, the analysis of the LEED intensities has not allowed to identify unequivocally the specific adsorption site(s) in that coverage range or at variable temperatures. Baró and Erley employed Electron Energy Loss Spectroscopy (EELS) to measure the vibrational frequencies of H atoms adsorbed on the Fe(110) surface. From the number of frequencies measured with EELS, one would in principle be able to determine the symmetry and therefore the type of adsorption site. Baró and Erley detected two peaks in the EELS spectra and concluded the lb site to be the preferential adsorption site for H on Fe(110) [21].

Initial theoretical work focused on simulating the various adsorption motifs as a function of coverage [22]. The first embedded cluster calculations by Muscat confirmed the existence of the $(2 \times 1)$, $(3 \times 1)$, $(1 \times 1)$, and also the $(2 \times 2)$ phase, and also pointed to the 3f site as the most stable adsorption site [23], but later concluded the short-bridge site to be the most favourable [22]. Raeker and DePristo later employed a corrected effective medium method

3

(CEM) which treats the surrounding surface atoms as jellium and, purely based on their similar adsorption energies, concluded the 3f and long-bridge site to be similarly stable [24]. Cremaschi *et al.* performed *ab initio* configuration interaction calculations to derive very similar adsorption energies for all three binding sites, and calculated the stretching frequency of H on the 3f site of Fe(110) to be $1073\,\mathrm{cm}^{-1}$ [25]. Jiang and Carter performed DFT calculations of H on Fe(110) [26], focussing on the $(2 \times 1)$ and $(2 \times 2)$-2H structures. They confirmed the 3f adsorption site to be the most stable, not only due to it being the lowest in energy (if only by a small margin), but mainly due to their vibrational analysis: only the 3f site is a true minimum, whereas all other sites have at least one imaginary frequency, making the sb and lb site transition states to the 3f minimum (and the ot site a rank-two saddle point). The harmonic frequency of the stretching vibration perpendicular to the surface was calculated to be at $1063\,\mathrm{cm}^{-1}$ (at $25\,\%$ coverage), while the frustrated translations display harmonic frequencies of 740 and $954\,\mathrm{cm}^{-1}$ (at $50\,\%$ coverage). Following this, a H diffusion study into and through the bulk of Fe was conducted. It was found that H hops from tetrahedral to tetrahedral site, along a curved trajectory from the surface towards the bulk. However it was noted that H prefers to remain on the surface, and that the entire diffusion process is endothermic [27, 28]. Kristinsdóttir and Skúlason conducted a surface diffusion study of H on various transition metal surfaces, including the Fe(110) surface [29]. They deduced a critical temperature for diffusion of $-214\,^{\circ}\mathrm{C}$, and an activation barrier of $0.18\,\mathrm{eV}$ for diffusion. Xie *et al.* calculated the adsorption process for $H_2$ on Fe(110) [30]. They found that the $H_2$ binds weakly to the surface, and that it dissociates into H atoms, which bind to the surface. Most recently, Wang *et al.* used *ab initio* thermodynamics to compute the desorption energy of $H_2$ at finite temperature as on various Fe surfaces, including the (110) surface [31]. The (110) plane was found to be the most prominently exposed surface at $402\,^{\circ}\mathrm{C}$, and that $H_2$ desorbs from the (110) plane at $57\,^{\circ}\mathrm{C}$, with a desorption energy of $1.0\,\mathrm{eV}$ per $H_2$.

In this paper, we report a systematic study of the adsorption of hydrogen on the bcc Fe(110) surface as a function of the degree of coverage, based on density functional theory (DFT), including a complete vibrational analysis and the surface magnetocrystalline effects. We expect that this work will prompt an accelerated search for effective gas additives [32, 33] or coatings [34, 35] to inhibit the hydrogen-induced embrittlement in these materials, and will also stimulate new experimental attempts to measure the vibrational frequencies with high resolution, by performing state-of-the-art EELS experiments, or non-linear surface-spectroscopic laser experiments at wavenumbers of around $1000\,\mathrm{cm}^{-1}$ and below [36, 37].

4

## 2. Methodology

We have performed first principles quantum mechanical calculations based on the spin-polarised density-functional theory (DFT) using the Cambridge Serial Total Energy Package (CASTEP). This software package solves the Kohn-Sham equations with a plane wave basis set employing three-dimensional periodic boundary conditions [38]. We employed the Perdew–Burke–Ernzerhof (PBE) version of the generalized gradient approximation (GGA) to represent the exchange and correlations [39], and on-the-fly ultrasoft pseudopotentials for Fe and H. The Monkhorst–Pack (MP) algorithm was selected for $k$-point sampling [40]. For bulk bcc Fe, a cut-off energy of $750\,\text{eV}$ and an $8 \times 8 \times 8$ MP grid size was found to converge the total energy of the system. Using those parameters and the Broyden–Fletcher–Goldfarb–Shanno (BFGS) algorithm [41], where the forces were minimised to within $0.05\,\text{eV}\,\text{Å}^{-1}$, we derived the lattice parameter, $a$, for bulk bcc Fe. A Gaussian smearing with a width of $0.1\,\text{eV}$ applies an artificial electronic temperature to describe partial occupancies about the Fermi level. Furthermore, the local magnetic moment of Fe, $\mu$, was approximated using the Mulliken population analysis [42].

A six-layer slab model with a vacuum gap of $20\,\text{Å}$ was used to represent the Fe(110) surface. We selected a MP grid size of $16 \times 8 \times 1$, and the $k$-point sampling was kept constant for other cell geometries by rescaling the MP grid size accordingly. We used the BFGS algorithm to relax the positions of the Fe atoms in the top three layers, whilst the bottom three layers were constrained. The relaxation was computed using the relationship

$$\Delta_{ij}(\%) = 100 \times \left( \frac{d_{ij} - d_0}{d_0} \right) \tag{1}$$

where $d_{ij}$ is the interlayer spacing between two adjacent Fe layers $i$ and $j$ (where $j = i + 1$), and $d_0$ is the bulk spacing. The surface energy, $\gamma$, was then obtained using the equation

$$\gamma = \frac{E_\text{slab} - n\,E_\text{bulk}}{2A} \tag{2}$$

where $A$ is the cross-sectional area of the slab, $E_\text{slab}$ is the total energy of the slab, $n$ is the number of Fe atoms in the slab and $E_\text{bulk}$ is the energy of a single Fe atom in the bulk. The Fe magnetic moment in the individual layers, $\mu_i$, was also estimated based on the Mulliken population analysis. Hydrogen was then adsorbed on each of the four potential sites on the bcc Fe(110) surface, for representative cell geometries and degrees of coverage. The top three layers of Fe were still allowed to relax, with the H atoms free to move. Using the relaxed geometry, the adsorption energy was computed for each case to find the most stable

5

site. The adsorption energy, $E_{\text{ads}}$ is given by

$$E_{\text{ads}} = \frac{1}{N} \left[ E_{\text{H+slab}} - (N E_{\text{H}} + E_{\text{slab}}) \right] \tag{3}$$

where $E_{\text{H+slab}}$ is the total energy of the relaxed slab with H adsorbed, $N$ is the number of adsorbed H atoms, $E_{\text{H}}$ is the ground state energy of a single H atom, and $E_{\text{slab}}$ is the total energy of the H-free slab. The potential energy surface (PES) was calculated along a pathway connecting the four adsorption sites. The top three Fe layers were allowed to relax, and the H atom allowed to relax normal to the (110) plane. The energy was evaluated at various H locations between the four potential adsorption sites. The energies were calculated relative to the starting point in each potential diffusion pathway. A frozen mode finite displacement calculation was subsequently used to compute the vibrational frequencies of the surface-adsorbed H atoms in each case. A finite displacement of $0.01\,\text{Å}$ on the H atoms was applied to compute the force constant matrix, from which the vibrational frequencies were calculated.

The spin-polarised projected density of states (PDOS) were calculated using the OP-TADOS code [43]. An adaptive smearing with width $0.4\,\text{eV}$ was applied [44]. The PDOS was integrated to compute the difference in the spin-up ($N_\uparrow$) and spin-down ($N_\downarrow$) valence electrons, i.e.

$$\Delta N = N_\uparrow - N_\downarrow = \int_{-\infty}^{0} (n^+(E) - n^-(E)) dE \tag{4}$$

where $n^+$ and $n^-$ (abbreviated as $n^\pm$) is the PDOS for the spin-majority (+) and minority (-) states, respectively. Furthermore, the $d$-band centre, $c_d^\pm$, and $d$-band width, $w_d^\pm$, for spin-majority and minority states were computed via the relations [45]

$$c_d^\pm = \frac{\int_{-\infty}^{\infty} E\, n^\pm(E) dE}{\int_{-\infty}^{\infty} n^\pm(E) dE} \tag{5}$$

and

$$w_d^\pm = \left( \frac{\int_{-\infty}^{\infty} E^2\, n^\pm(E) dE}{\int_{-\infty}^{\infty} n^\pm(E) dE} \right)^{\frac{1}{2}}. \tag{6}$$

These quantities were averaged to give the $d$-band centre, $c_d$, and $d$-band width, $w_d$, i.e. $c_d = (c_d^+ + c_d^-)/2$ and $w_d = (w_d^+ + w_d^-)/2$.

## 3. Results

### 3.1. Hydrogen-free Fe(110) surface

The lattice parameter ($a = 2.837\,\text{Å}$) of bulk bcc Fe derived from our DFT modelling is in good agreement with the reported experimental value ($a = 2.86\,\text{Å}$) [46], as well as previous

6

DFT studies (in the range of 2.83 to 2.91 Å) [26, 27, 29, 30, 31, 47]. The derived value of the bulk interlayer spacing ($d_0$) is 2.02 Å. We found a value of the Fe magnetic moment of $2.22\,\mu_\mathrm{B}$/atom, which coincides with the experimentally measured magnetic moment of $2.22\,\mu_\mathrm{B}$/atom [48] as well as previous DFT calculations (from 2.20 to $2.22\,\mu_\mathrm{B}$/atom) [26, 27, 31, 47]. Once we had modelled reliably the bulk bcc Fe characteristics, we proceeded to compute the relaxation, surface energy and magnetic moment of a six layer H-free slab of Fe(110) for selected cell geometries using spin-polarised DFT. We did not observe any significant structural reconstruction at or close to the H-free surface, only a relatively small relaxation normal to the surface between the top three Fe layers relative to the bulk. The spacing between the first and second layer reduces relative to the bulk interlayer spacing, i.e. $\Delta_{12} = -0.37\,\%$. This effect is compensated by an expansion between the second and third layer $\Delta_{23} = 0.57\,\%$. These values come close to the experimental values of $\Delta_{12} = 1(2)\,\%$ and $\Delta_{23} = 0.5(1.0)\,\%$ [49]. They also agree with the previous calculated values of $\Delta_{12}$ and $\Delta_{23}$ using DFT, ranging from $-0.62$ to $0\,\%$ and 0.26 to $0.89\,\%$, respectively [26, 50, 51, 52, 53]. The surface energy takes a value of $\gamma = 2.47\,\mathrm{J\,m^{-2}}$, in close agreement with the experimental value of $2.48\,\mathrm{J\,m^{-2}}$ [54] as well as calculated values of 2.43 and $2.41\,\mathrm{J\,m^{-2}}$ using DFT [26, 50].

Our results also reveal an increased Fe magnetic moment at the surface relative to the bulk, with a value in the first layer of $\mu_1 = 2.68\,\mu_\mathrm{B}$/atom. This corresponds to an enhancement of $\sim 21\,\%$ with respect to the bulk, in reasonable agreement with the enhancement observed experimentally of $39(16)\,\%$ relative to the bulk, corresponding to a value of $3.08\,\mu_\mathrm{B}$ per atom [55]. This is also close to values obtained in previous DFT investigations, of 2.74 and $2.58\,\mu_\mathrm{B}$ per atom [26, 50]. Fe is described as an itinerant-electron ferromagnet, whose magnetization stems from the spin polarisation of the itinerant $d$-electrons. The nearest-neighbour interactions seem to control the $d$-band width. At the bcc-Fe surface, the coordination number reduces from eight to six, and this leads to a smaller band width and consequently a higher magnetization [56, 57]. From our calculations, the $d$-band width is 3.11 eV in bulk, whilst the $d$-band width is 2.85 and 3.03 eV in the first and second layers, respectively. Experimental results on magnetic step moments confirm the intermediate position of the Fe surface magnetism with respect to the bulk and the free atom behaviour [48]. The enhanced magnetism is still present in the second layer, but lies closer to the bulk properties ($\mu_2 = 2.30\,\mu_\mathrm{B}$/atom). The bulk value is reached at the third layer, i.e. $\mu_3 = 2.22\,\mu_\mathrm{B}$/atom.

## 3.2. H adsorbed on the Fe(110) surface

### 3.2.1. Site-specific adsorption energy

We have calculated the adsorption energies of atomic hydrogen at the four potential sites on the Fe(110) surface for representative coverages, see Table 1. The adsorbed H-Fe(110) cell geometries corresponding to the selected degrees of coverage are depicted in Fig. 2. Our results reveal that the 3f site is the thermodynamically most stable site, although the lb site is close in energy. The two-fold sb site and especially the ot site are energetically less favourable for all studied degrees of coverage. Additionally, we observe a reduction in the adsorption energy for the four potential sites for higher coverages. This reduction may stem from the increasing repulsive interactions between co-adsorbed H atoms over that coverage range [26]. In order to further understand the relative energetics in between the adsorption sites, the potential energy surface (PES) was calculated along the pathways connecting the four high symmetry sites; we used the $(4 \times 1)$ cell for this procedure. The resulting plots are shown in Fig. 3. From Fig. 3 a and b, it is clear that the ot site is highly unstable. Similarly, the data in Fig. 3 c and d, reveal that the 3f site is more stable than the lb and sb sites.

The calculated values of the equilibrium H-to-surface distance and the corresponding H-Fe bond length are collected in Table 2. These two distances are identical for the ot case where the H atom resides directly above an iron atom, whilst it would be located above and between multiple atoms in the other three cases. It is worth noting that the average H-to-surface distance takes the smallest value, i.e. $0.95(3)\,\text{Å}$, when the H atoms reside on either the 3f or the lb site. This confirms the relative instability of the H occupancy of the ot and sb sites with respect to the lb and 3f sites. The reported value for the 3f H-to-surface distance of $0.9(1)\,\text{Å}$, determined using LEED [58], is in good agreement with our calculated value of $0.91\,\text{Å}$ for a H coverage of $100\,\%$.

### 3.2.2. Vibrational analysis

A vibrational study of H on Fe(110) on the four sites was conducted, shown in Table 3. We have found two imaginary frequencies for the ot site, and is thus a rank-two saddle point. The sb and lb sites have single imaginary frequencies, hence they are transition states. The 3f site has three real frequencies, and is thus a true minimum. This data is concordant with our prior study of the potential energy surfaces in between adsorption sites (section 3.2.1). For similar phonon calculations for the $(2 \times 1)$ and $(1 \times 1)$ geometries, corresponding to 50 and $100\,\%$, we found the same order of stability at all four adsorption sites. Having established that the 3f site is the most stable adsorption site, it will be further considered in the vibrational frequency analysis for variable degrees of coverage.

There are three vibrational modes for adsorption of H on the 3f site of Fe(110): two frustrated translational modes parallel to the (110) plane ($\tilde{\nu}_{t1}$, which is along [1$\bar{1}$0], and $\tilde{\nu}_{t2}$ along [001]), and a stretch vibrational mode ($\tilde{\nu}_s$), see Fig. 4. We have determined the 3f vibrational frequencies for representative degrees of coverage in the range of 25 to 100 %, see Table 4. The stretching mode naturally appears at higher frequencies than the two frustrated translational modes. We also observe a clear increase in the vibrational frequency with the degree of coverage. The $\tilde{\nu}_{t1}$ vibration along the [1$\bar{1}$0] direction spans from 736 to 953 cm$^{-1}$, whilst the $\tilde{\nu}_{t2}$ vibration along the [001] direction ranges from 925 to 1014 cm$^{-1}$ depending on coverage. For those coverages that require two hydrogen atoms per unit cell in our simulations, we obtain two values for $\tilde{\nu}_{t1}$ and $\tilde{\nu}_{t2}$ each (50 % and 67 %). The first frequency $\tilde{\nu}_{t1}$ represents the alternating oscillation of the H atoms, while the second frequency $\tilde{\nu}_{t2}$ stems from the concurrent oscillation. These two values are generally close in magnitude, since they are both in the same plane and originate from similar forces. We hope that these DFT results can motivate future high-resolution EELS experiments or non-linear laser-spectroscopic surface experiments to unequivocally identify the two frustrated translation modes experimentally, and their dependence on environmental conditions such as hydrogen pressure and/or temperature.

### 3.2.3. Hydrogen-induced magnetocrystalline effects

The adsorption of hydrogen atoms on metallic surfaces can induce significant changes in the surface structure and magnetism [59]. We have studied the effect of H-Fe(110) adsorption on the normal relaxation and surface Fe magnetic moment as we increase the degree of H coverage. At very low coverage, our study reveals that the H atoms occupy the high-coordination 3f sites and behave like a lattice gas. This H adsorption process induces local displacements of the (near-) surface Fe atoms in the vicinity of the occupied 3f sites. As a consequence, the contraction of the first-to-second layer distance, initially present in the H-free surface, gradually decreases. Moreover, the H atoms tend to push the neighbouring Fe atoms inwards into the bulk, and this induces a buckling phenomenon. This effect is characterised by the buckling parameter, $b_i$, for each of the three near-surface Fe layers ($i$ = 1, 2, 3), see Fig. 5. The variation of $\Delta_{12}$ and $b_1$ with H coverage is shown in Fig. 6 a. At the lowest coverage of 25 %, corresponding to the Fe(110)-(4 × 1)-H superstructure, the fairly isolated H atoms cause the displacement of surrounding Fe atoms, corresponding to the maximum buckling parameter in this study of $b_1 = 0.058$ Å.

A similar buckling effect also takes place in the second and third layer, but its magnitude is reduced with respect to the effect in the first layer: at $\theta_H = 25$ %, the second and third

layer buckling parameters are $b_2 = 0.022\,\text{Å}$ and $b_3 = 0.012\,\text{Å}$, respectively. It is also worth stressing that at this H coverage, the first-to-second layer distance is expanded with respect to the bulk value, i.e. $\Delta_{12}$ is now positive, whereas it is negative in the absence of any adsorbents. Surface relaxation is significant for all hydrogen coverages studied but is least pronounced for a 25 % coverage; buckling, however, is most pronounced at 25 % coverage and decreases rapidly towards higher coverages, in fact it is almost negligible for coverages of 50 % and higher. The implication of both the increased interlayer spacing $d_{12}$ for most coverages and increased buckling with hydrogen adsorption for 25 % and 33 % is (a) less steric hindrance for hydrogen atoms between the first and second layer, and (b) the availability of more sub-surface adsorption sites due to buckling, both of which may lead to enhanced hydrogen diffusion into the bulk.

The presence of chemisorbed hydrogen on Fe(110) is also expected to influence the magnetism of the surface Fe atoms [60]. Fig. 6 b shows the variation of the Fe magnetic moment in the first and second layer, $\mu_1$ and $\mu_2$, with the degree of coverage. Our results show a continuous decrease in the magnetic moment of the first layer, reducing from $2.68\,\mu_\text{B}/\text{atom}$ in the H-free surface to $2.46\,\mu_\text{B}/\text{atom}$ for $\theta_\text{H} = 100\,\%$. The formation of H-Fe surface bonds increases the coordination number of the surface Fe atoms, which gradually shifts the surface magnetic moment towards the bulk value. In parallel to the decrease in $\mu_1$, we also observe an increase in the Fe moment in the second layer, $\mu_2$, however, the magnitude of this effect is significantly smaller than the observed decrease in $\mu_1$, and only amounts to $\sim 5\,\%$. This change can be explained by monitoring the changes in the PDOS, as a function of coverage. These changes are quantified using the $d$-band width, $w_d$, $d$-band centre, $c_d$, and difference in spin-up and spin-down valence electrons, $\Delta N$, see Fig. 7 . There is a clear reduction in $\Delta N$ as a function of coverage in the first layer with increasing coverage, whilst the converse is true for the second layer. The shift in this quantity is related to the Fe magnetic moment by $\mu = \Delta N \mu_\text{B}$ [61]. In agreement with the observed trend in the $\Delta N$, the $d$-band width increases with coverage in the first layer, whilst there is negligible change in the second layer. Further to this, there is a linear relation between the adsorption energy and the $d$-band centre, as shown in Fig. 7 f. Collectively, this indicates that the adsorbate-metal system is well modelled by the $d$-band model, as posed by Hammer and Nørskov [62]. Furthermore, for increasing coverage, there is increasing hybridisation between the $s$ orbital of H and the $d$-band of Fe, resulting in a more strongly chemisorbed H adsorbate on the surface. A characteristic of this is the increased PDOS for the hydrogen atom, in between 25 and 100 % coverage. There is coupling between the Fe and H orbitals as the PDOS takes

a similar form between $-4$ and $-6\,\mathrm{eV}$, relative to the Fermi level, $E_\mathrm{F}$, at $100\,\%$ coverage, see Fig. 7 c.

## 4. Conclusions

We have studied the hydrogen adsorption on the (110) surface of bcc Fe, and its effect on the local atomic arrangement and magnetic moment, by performing first principle calculations as a function of the hydrogen coverage. We found the quasi-threefold (3f) site to be the most stable site for the H to reside, with adsorption energies of $\sim 3.0\,\mathrm{eV/H}$ for all coverages studied. The lb and sb sites constitute transition state that lead to the stable 3f site, as deduced from the fact that H in those sites has a single imaginary vibrational frequency. We calculated the harmonic vibrational frequencies for hydrogen adsorption at the 3f site for cell geometries and coverages studied. The symmetric stretch vibration appears at wavenumbers ranging from 1070 to $1095\,\mathrm{cm^{-1}}$ for H coverages below $50\,\%$, while the two frustrated translational modes parallel to the (110) plane appear at lower energies (730 to $1015\,\mathrm{cm^{-1}}$). The H adsorption on the 3f site induces local distortions on the arrangement of Fe atoms, namely a buckling effect in the surface Fe layers that is most pronounced in the first layer for a $25\,\%$ coverage. Additionally, H adsorption also causes an expansion of the first-to-second layer distance with respect to the bulk, and concomitantly a gradual reduction of the Fe magnetic moment in the first layer towards the bulk Fe moment with increasing H coverage. This will impact the modelling of H diffusion into the bulk, since the atomic re-arrangements will imply less steric hindrance and more sub-surface adsorption sites for the H atoms. We also hope that these results will motivate future high-resolution surface spectroscopy studies, and that our work will advance the mechanistic understanding and prediction of the early stages in the hydrogen embrittlement of ferritic steels.

# References

[1] L. Schlapbach, A. Züttel, Hydrogen-storage materials for mobile applications, Nature Mater. 414 (2001) 353–358.

[2] P. Rhodes, L. Skogsberg, R. Tuttle, Pushing the Limits of Metals in Corrosive Oil and Gas Well Environments, Corrosion 63 (2007) 63–100.

[3] S. Pimblott, J. Laverne, Radiation chemistry of water in contact with nuclear fuels and structural materials, Trans. Am. Nucl. Soc. 102 (2010) 777.

[4] W. Oates, T. Flanagan, The solubility of hydrogen in transition metals and their alloys, Prog. Solid State Chem. 13 (1981) 193–283.

[5] M. Louthan Jr, Hydrogen Embrittlement of Metals: A primer for the Failure Analyst, J. Fail. Anal. and Preven. 8 (2008) 289–307.

[6] S. Lynch, Hydrogen embrittlement phenomena and mechanisms, Corros. Rev. (2012) 105–123.

[7] P. Fassina, M. Brunella, L. Lazzari, G. Re, L. Vergani, A. Sciuccati, Effect of hydrogen and low temperature on fatigue crack growth of pipeline steels, Eng. Fract. Mech. 103 (2013) 10–25.

[8] D. Hardie, E. Charles, A. Lopez, Hydrogen embrittlement of high strength pipeline steels, Corros. Sci. 48 (2006) 4378–4385.

[9] T. Michler, J. Naumann, Microstructural aspects upon hydrogen environment embrittlement of various bcc steels, Int. J. Hydrog. Energy 35 (2010) 821–832.

[10] J. Marques, Evolution of nuclear fission reactors: Third generation and beyond, Energy Conv. Manag. 51 (2010) 1774–1780.

[11] S. Zinkle, N. Ghoniem, Prospects for accelerated development of high performance structural materials, J. Nucl. Mater. 417 (2011) 2–8.

[12] H. Bhadeshia, R. Honeycombe, Steels: Microstructure and Properties, 3rd Edition, Butterworth-Heinemann, 2006.

[13] J. Savoie, R. K. Ray, M. P. Butrón-Guillén, J. J. Jonas, Comparison between simulated and experimental transformation textures in a Nb microalloyed steel, Acta Metall. Mater. 42 (1994) 2511–2523.

[14] G. A. Samorjai, Y. Li, Introduction to surface chemistry and catalysis, 2nd Edition, John Wiley & Sons, 2010.

[15] K. Christmann, Interaction of hydrogen with solid surfaces, Surf. Sci. Rep. 9 (1988) 1–163.

[16] F. Bozso, G. Ertl, M. Grunze, M. Weiss, Chemisorption of hydrogen on iron surfaces 1 (1977) 103–119.

[17] K. Yoshida, Adsorption of $H_2$ on (110), (111) and Stepped (111) Iron Single Crystal Surfaces, Japan. J. Appl. Phys. 19 (1980) 1873–1883.

[18] J.-P. Muscat, Role of multi-adatom interactions in the formation of ordered structures on metal surfaces: Application to H/Fe (110), Surf. Sci. 139 (1984) 491–504.

[19] R. Imbihl, R. J. Behm, K. Christmann, G. Ertl, T. Matsushima, Phase transitions of a two-dimensional chemisorbed system: H on Fe (110), Surf. Sci. 117 (1982) 257–266.

[20] W. Nichtl-Pecher, J. Gossmann, L. Hammer, K. Heinz, K. Müller, Adsorption of hydrogen on Fe (110) at cryogenic temperatures investigated by low energy electron diffraction, J. Vac. Sci. & Technol. A 10 (1992) 501–507.

[21] A. M. Baró, W. Erley, The chemisorption of hydrogen on a (110) iron crystal studied by vibrational spectroscopy (EELS), Surf. Sci. Lett. 112 (1981) L759–L764.

[22] W. Kinzel, W. Selke, K. Binder, Phase transitions on centred rectangular lattice gases: A model for the adsorption of H on Fe (110), Surf. Sci. 121 (1982) 13–31.

[23] J.-P. Muscat, Pair interaction energies for H adsorbed on Fe (110), Surf. Sci. 118 (1982) 321–328.

[24] T. J. Raeker, A. E. DePristo, Corrected effective medium calculations of the chemisorption of H and N on Fe (100), Fe (110) and W (110), Surf. Sci. 235 (1990) 84–106.

[25] P. Cremaschi, H. Yang, J. L. Whitten, Ab initio chemisorption studies of H on Fe (110), Surf. Sci. 330 (1995) 255–264.

[26] D. Jiang, E. A. Carter, Adsorption and diffusion energetics of hydrogen atoms on Fe (110) from first principles, Surf. Sci. 547 (2003) 85–98.

[27] D. Jiang, E. A. Carter, Diffusion of interstitial hydrogen into and through bcc Fe from first principles, Phys. Rev. B 70 (2004) 064102(1)–064102(9).

[28] P. Ferrin, S. Kandoi, A. U. Nilekar, M. Mavrikakis, Hydrogen adsorption, absorption and diffusion on and in transition metal surfaces: A DFT study, Surf. Sci. 606 (2012) 679–689.

[29] L. Kristinsdóttir, E. Skúlason, A systematic DFT study of hydrogen diffusion on transition metal surfaces, Surf. Sci. 606 (2012) 1400–1404.

[30] W. Xie, L. Peng, D. Peng, F. L. Gu, J. Liu, Processes of $H_2$ adsorption on Fe (110) surface: A density functional theory study, Appl. Surf. Sci. 296 (2014) 47–52.

[31] T. Wang, S. Wang, Q. Luo, Y.-W. Li, J. Wang, M. Beller, H. Jiao, Hydrogen adsorption structures and energetics on iron surfaces at high coverage, J. Phys. Chem. C 118 (2014) 4181–4188.

[32] V. Srikrishnan, P. J. Ficalora, The Role of Gaseous Impurities in the Hydrogen-embrittlement of Steel, J. Vac. Sci. Technol. 14 (1977) 588–592.

[33] K. Kussmaul, P. Deimel, H. Fischer, E. Sattler, Fracture mechanical behaviour of the steel 15MnNi 6 3 in argon and in high pressure hydrogen gas with admixtures of oxygen, Int. J. Hydrog. Energy 23 (1998) 577–582.

[34] K. Forsey, D. Ross, C. Wu, The Formation of Hydrogen Permeation Barriers on Steels by Aluminising, J. Nucl. Mater. 182 (1991) 36–51.

[35] T. H. Nam, J. H. Lee, S. R. Choi, J. B. Yoo, J. G. Kim, Graphene coating as a protective barrier against hydrogen embrittlement, Int. J. Hydrog. Energy 39 (2014) 11810–11817.

[36] C. Williams, Y. Yang, C. Bain, Prospects for detecting metaladsorbate vibrations by sum-frequency spectroscopy, Catal. Lett. 61 (1999) 7–13.

[37] A. B. Sugiharto, C. M. Johnson, H. B. De Aguiar, L. Alloatti, S. Roke, Generation and application of high power femtosecond pulses in the vibrational fingerprint region, Appl. Phys. B 91 (2008) 315–318.

[38] S. J. Clark, I. Matthew, D. Segall, C. J. Pickard, P. J. Hasnip, M. I. J. Probert, K. Refson, M. C. Payne, First principles methods using CASTEP, Z. Kristallogr. 220 (2005) 567–570.

[39] J. P. Perdew, K. Burke, M. Ernzerhof, Generalized Gradient Approximation Made Simple, Phys. Rev. Lett. 77 (1996) 3865–3868.

[40] J. D. Pack, H. J. Monkhorst, Special points for Brilluoin-zone integrations, Phys. Rev. B 13 (1976) 5188–5192.

[41] B. G. Pfrommer, M. Côté, S. G. Louie, M. L. Cohen, Relaxation of crystals with the quasi-Newton method, J. Comput. Phys. 131 (1997) 233–240.

[42] R. Mulliken, Electronic Population Analysis on LCAO-MO Molecular Wave Functions. I, J. Chem.

13

Phys. 23 (1955) 1833–1840.

[43] A. J. Morris, R. Nicholls, C. J. Pickard, J. Yates, OptaDOS: A tool for obtaining density of states, core-level and optical spectra from electronic structure codes, Comp. Phys. Comm. 185 (2014) 1477.

[44] J. R. Yates, X. Wang, D. Vanderbilt, I. Souza, Spectral and Fermi surface properties from Wannier interpolation, Phys. Rev. B 75 (2007) 195121.

[45] P. Kratzer, B. Hammer, J. Nørksov, A theoretical study of $CH_4$ dissociation on pure and gold-alloyed Ni (111) surfaces, J. Chem. Phys 105 (1996) 5595–5604.

[46] C. Kittel, Introduction to Solid State Physics, 7th Edition, John Wiley & Sons, 1996.

[47] A. Stibor, G. Kresse, A. Eichler, J. Hafner, Density functional study of the adsorption of CO on Fe (110), Surf. Sci. 507 (2002) 99–102.

[48] M. Albrecht, T. Furubayashi, U. Gradmann, W. Harrison, Magnetic step moments, J. Magn. Magn. Mater. 104 (1992) 1699–1670.

[49] C. Xu, D. O'Connor, Surface relaxation trend study with iron surfaces, Nucl. Instr. Meth. Phys. Res. B 53 (1991) 315–325.

[50] Błoński, P and Kiejna, A and Hafner, J, Theoretical study of oxygen adsorption at the Fe (110) and (100) surfaces, Surf. Sci. 590 (2005) 88–100.

[51] Pick, Štěpán and Légaré, Pierre and Demangeat, Claude, Density-functional study of the chemisorption of N on and below Fe (110) and Fe (001) surfaces, Phys. Rev. B 75 (2007) 195446.

[52] Tan, Xiaochao and Zhou, Jicheng and Peng, Yinqiao, First-principles study of oxygen adsorption on Fe (110) surface, Appl. Surf. Sci. 258 (2012) 8484–8491.

[53] Mortensen, Jens Jørgen and Ganduglia-Pirovano, MV and Hansen, Lars Bruno and Hammer, Bjørk and Stoltze, Per and Nørskov, Jens Kehlet, Nitrogen adsorption on Fe (111),(100), and (110) surfaces, Surf. Sci. 422 (1999) 8–16.

[54] L. Vitos, A. Ruban, H. L. Skriver, J. Kollar, The surface energy of metals, Surf. Sci. 411 (1998) 186–202.

[55] K. Wagner, N. Weber, H. Elmers, U. Gradmann, Magnetization of free Fe (110) surfaces from thin film magnetometry, J. Magn. Magn. Mater. 167 (1997) 21–26.

[56] R. Victoria, L. Falicov, S. Ishida, Calculated surface electronic structure of ferromagnetic iron and the ferromagnetic ordered iron-cobalt alloy, Phys. Rev. B 30 (1984) 3896–3902.

[57] U. Gradmann, Surface magnetism, J. Magn. Magn. Mater. 100 (1991) 418–496.

[58] W. Moritz, R. Imbihl, R. J. Behm, G. Ertl, T. Matsushima, Adsorption geometry of hydrogen on Fe (110), J. Chem. Phys. 83 (1985) 1959–1968.

[59] K. Müller, Hydrogen-induced reconstruction of transition metal surfaces, Prog. Surf. Sci. 42 (1993) 245–255.

[60] W. Göpel, Magnetic dead layers on chemisorption at ferromagnetic surfaces, Surf. Sci. 85 (1979) 400–412.

[61] T.-S. Choy, J. Chen, S. Hershfield, Correlation between spin polarization and magnetic moment in ferromagnetic alloys, J. Appl. Phys. 86 (1999) 562–564.

[62] B. Hammer, J. Nørskov, Electronic factors determining the reactivity of metal surfaces, Surf. Sci. 343 (1995) 211–220.

## Tables

**Table 1:** Calculated values of the adsorption energies ($E_{\mathrm{ads}}$/eV per H atom) at the four potential adsorption sites for representative cell geometries.

| Cell geometry $(\theta_{\mathrm{H}})$ | Current work | | | | Previous work[a] | | | |
|---|---|---|---|---|---|---|---|---|
| | **3f** | **lb** | **sb** | **ot** | **3f** | **lb** | **sb** | **ot** |
| $(1 \times 1)$ (100 %) | -2.91 | -2.76 | -2.65 | -1.92 | -2.91 | -2.77 | -2.65 | -1.95 |
| $(2 \times 2)$-3H (75 %) | -2.95 | -2.84 | -2.72 | -2.05 | — | — | — | — |
| $(3 \times 1)$-2H (67 %) | -2.96 | — | — | — | — | — | — | — |
| $(2 \times 2)$-2H (50 %) | -3.01 | — | — | — | — | — | — | — |
| $(2 \times 1)$ (50 %) | -2.99 | -2.95 | -2.78 | -2.20 | — | — | — | — |
| $(3 \times 1)$ (33 %) | -2.98 | -2.92 | -2.76 | -2.20 | — | — | — | — |
| $(4 \times 1)$ (25 %) | -2.98 | -2.94 | -2.77 | -2.20 | — | — | — | — |
| $(2 \times 2)$ (25 %) | -2.98 | -2.93 | -2.77 | -2.21 | -3.00 | -2.95 | -2.81 | -2.28 |

[a]Ref. [26]

**Table 2:** Equilibrium H-to-surface distance, together with the corresponding H-Fe bond length (in parentheses), for selected cell geometries and degrees of coverage. The values are in units of Å.

| | Site | Cell geometry$(\theta_{\mathrm{H}})$ | | | | | Average |
| --- | --- | --- | --- | --- | --- | --- | --- |
| | | $(1 \times 1)$ $(100\,\%)$ | $(2 \times 1)$ $(50\,\%)$ | $(3 \times 1)$ $(33\,\%)$ | $(4 \times 1)$ $(25\,\%)$ | $(2 \times 2)$ $(25\,\%)$ | |
| **Current work** | 3f | 0.91 (1.77) | 0.95 (1.78) | 0.96 (1.78) | 0.99 (1.79) | 0.96 (1.79) | 0.95(3) (1.78(1)) |
| | lb | 0.93 (1.70) | 0.91 (1.74) | 0.98 (1.73) | 0.97 (1.74) | 0.95 (1.74) | 0.95(3) (1.73(2)) |
| | sb | 1.14 (1.68) | 1.15 (1.68) | 1.14 (1.68) | 1.16 (1.69) | 1.15 (1.69) | 1.15(1) (1.68(1)) |
| | ot | 1.54 (1.54) | 1.56 (1.56) | 1.56 (1.56) | 1.55 (1.55) | 1.57 (1.57) | 1.55(1) (1.55(1)) |
| **Previous work**[a] | 3f | 0.90 (1.72) | — | — | — | 0.94 (1.78) | — |
| | lb | 0.92 (1.69) | — | — | — | 0.95 (1.74) | — |
| | sb | 1.13 (1.67) | — | — | — | 1.14 (1.69) | — |
| | ot | 1.53 (1.53) | — | — | — | 1.56 (1.56) | — |

[a]Ref. [26]

**Table 3:** Vibrational frequencies for the H-atoms adsorbed on all four sites on the Fe(110) surface, for the case of 25 % coverage on the $(4 \times 1)$ cell geometry.

| Site | $\tilde{\nu}/\mathrm{cm}^{-1}$ | | | Relative stability |
| --- | --- | --- | --- | --- |
| ot | $524i$ | $395i$ | 1759 | Rank-two saddle point |
| sb | $462i$ | 1177 | 1313 | Transition state |
| lb | $487i$ | 1107 | 1170 | Transition state |
| 3f | 744 | 970 | 1085 | Minimum |

**Table 4:** Vibrational frequencies for H-atoms located at the 3f adsorption site, for selected combinations of cell geometries and degrees of coverage ($\theta_H$).

| Cell geometry | $\theta_H/\%$ | $\tilde{\nu}/\mathrm{cm}^{-1}$ | | |
|:---:|:---:|:---:|:---:|:---:|
| | | $\tilde{\nu}_{t1}$ | $\tilde{\nu}_{t2}$ | $\tilde{\nu}_s$ |
| $(2 \times 2)$ | 25 | 736 | 925 | 1074 |
| $(4 \times 1)$ | 25 | 744 | 970 | 1085 |
| $(3 \times 1)$ | 33 | 753 | 954 | 1093 |
| $(2 \times 1)$ | 50 | 753 | 972 | 1089 |
| $(2 \times 2)$-2H | 50 | 747/772 | 924/942 | 1086/1095 |
| $(3 \times 1)$-2H (far) | 67 | 791/816 | 962/969 | 1105/1106 |
| $(3 \times 1)$-2H (close) | 67 | 791/893 | 920/1015 | 1078/1180 |
| $(1 \times 1)$ | 100 | 953 | 1014 | 1218 |

# Figures
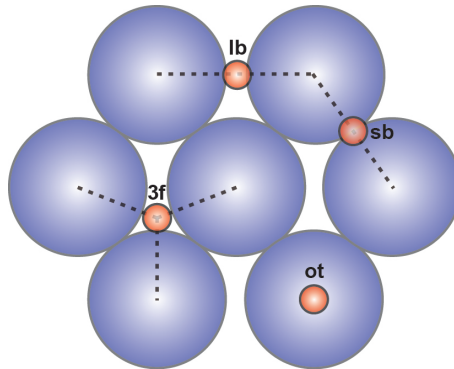


**Figure 1:** Potential adsorption sites for atomic hydrogen on the Fe(110) surface. ot = on-top, 3f = quasi-threefold, sb = short-bridge, lb = long-bridge.
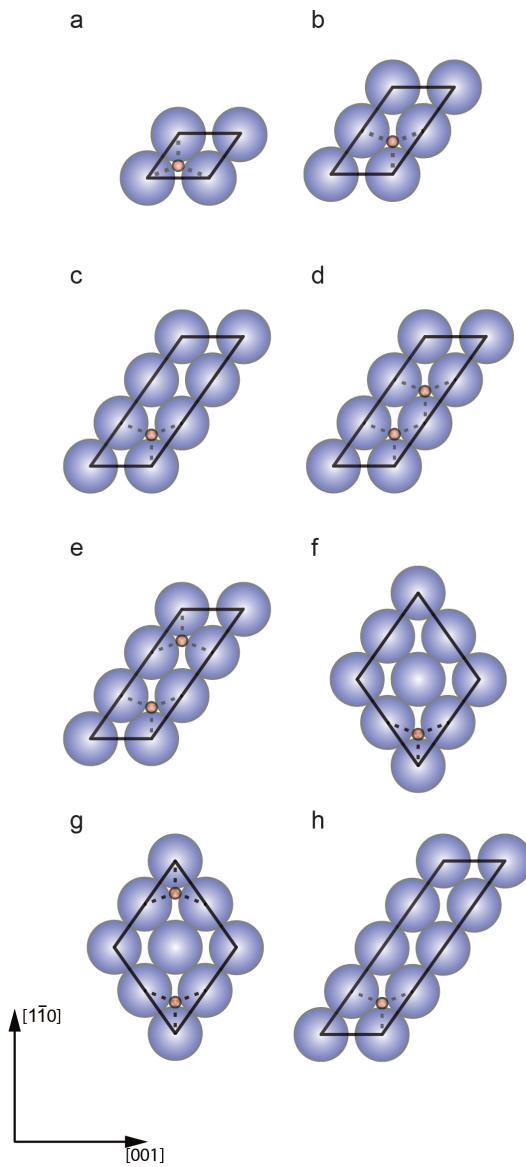
**Figure 2:** Adsorbed H-Fe(110) cell geometries and degree of coverage ($\theta_H$): (a) $(1 \times 1)$ ($\theta_H = 100\,\%$), (b) $(2 \times 1)$ ($\theta_H = 50\,\%$), (c) $(3 \times 1)$ ($\theta_H = 33\,\%$), (d) $(3 \times 1)$-2H (close) ($\theta_H = 67\,\%$), (e) $(3 \times 1)$-2H (far) ($\theta_H = 67\,\%$), (f) $(2 \times 2)$ ($\theta_H = 25\,\%$), (g) $(2 \times 2)$-2H ($\theta_H = 50\,\%$), (h) $(4 \times 1)$ ($\theta_H = 25\,\%$). The H atom is depicted on the 3f site.
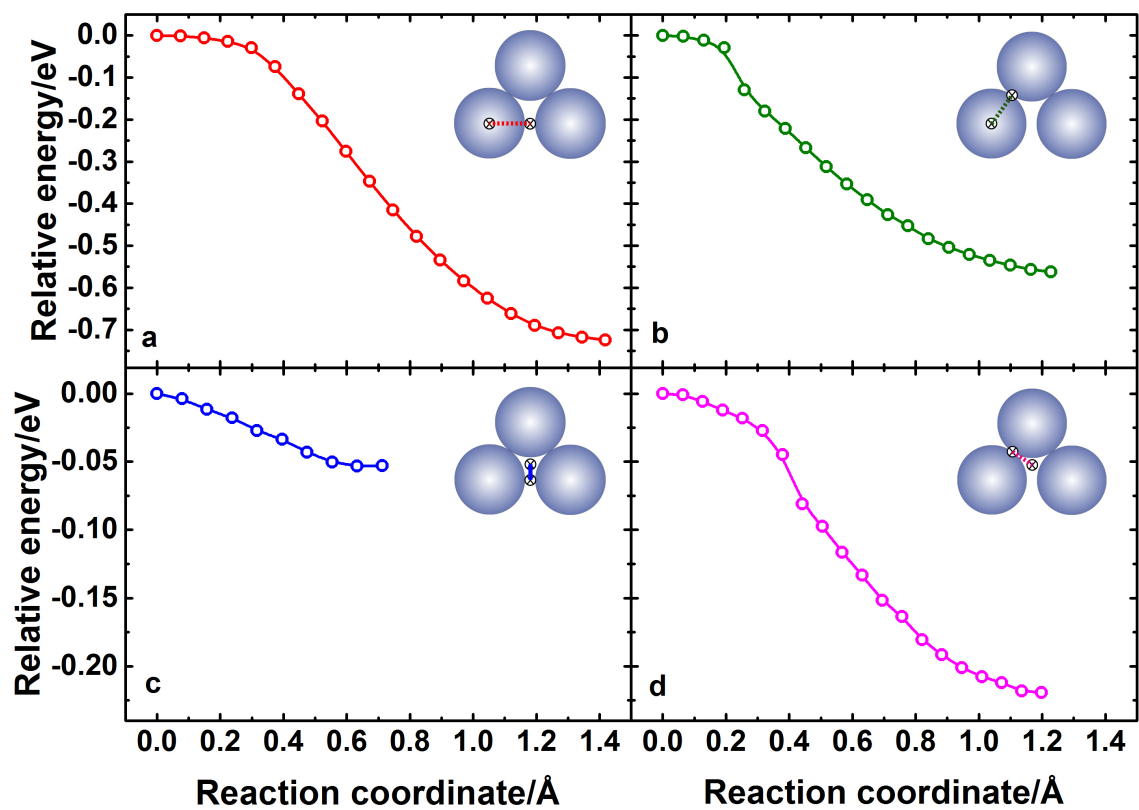
**Figure 3:** Potential energy surface between (a) ot-lb sites, (b) ot-sb sites, (c) lb-3f sites and (d) 3f-sb sites.
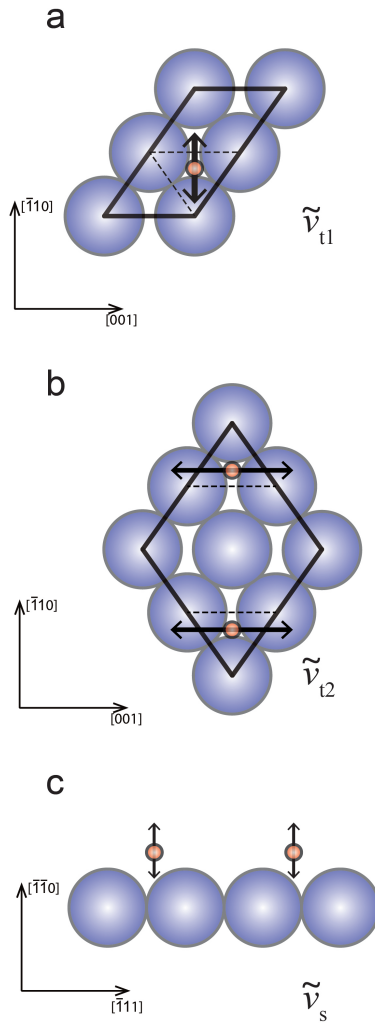
**Figure 4:** H-Fe vibrational modes: (a) First frustrated translation normal mode, $\tilde{\nu}_{t1}$ on $(2\times 1)$ $(\theta_H = 50\,\%)$, (b) Second frustrated translation normal mode, $\tilde{\nu}_{t2}$ on $(2 \times 2)$-2H $(\theta_H = 50\,\%)$, (c) Stretch vibration, $(\tilde{\nu}_s)$ on $(3 \times 1)$ $(\theta_H = 67\,\%)$
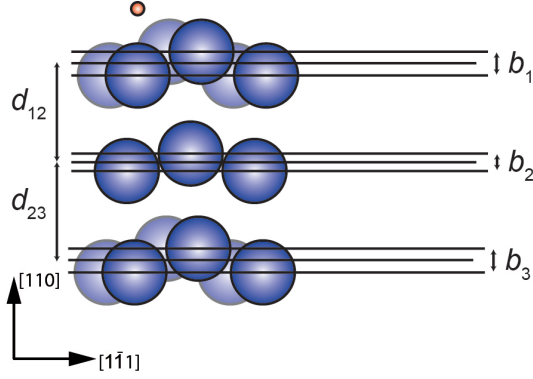
**Figure 5:** Schematic representation of the hydrogen-induced buckling reconstruction in the first three layers of the Fe slab, represented by the $b_i$ parameters, together with the inter-layer distances $d_{12}$ and $d_{23}$. The upper line and lower line are the highest and lowest positions of the atoms in a layer, respectively. The central line is the average of the position of the upper and lower lines.
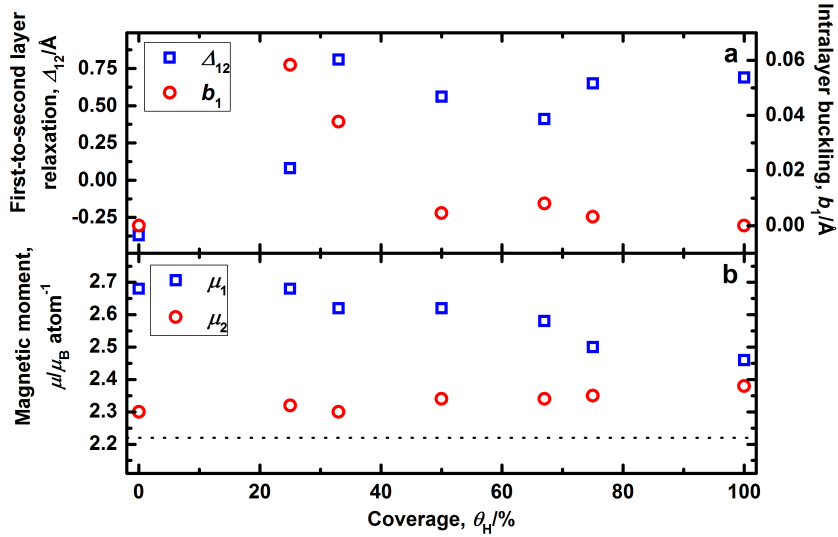


**Figure 6:** Variation of (a) the first-to-second layer relaxation ($\Delta_{12}$) and first-layer buckling ($b_1$), together with the magnetic moment per atom in the first ($\mu_1$) and second ($\mu_2$) layer, with the degree of hydrogen coverage ($\theta_H$). The horizontal dashed line in (b) represents the Fe bulk magnetic moment.
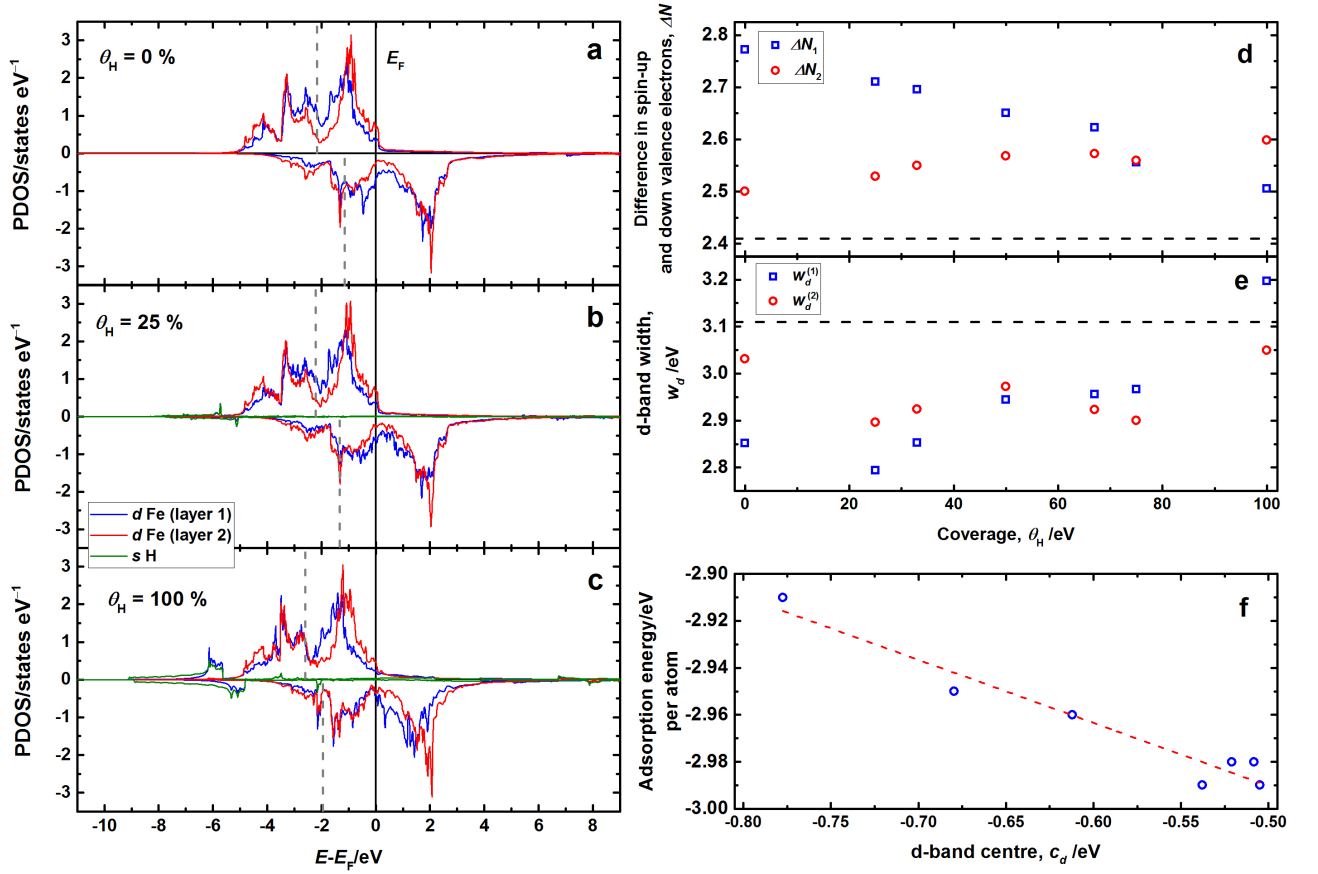
**Figure 7:** Spin-polarised projected density of states (PDOS) for three degrees of H-coverage: (a) 0 % coverage, (b) 25 % coverage, (c) clean geometry (100 % coverage). The three calculated parameters for all geometries from the PDOS are: (d) difference in spin-up and spin-down valence electrons, $\Delta N_i$, (e) $d$-band width, $w_d^{(i)}$ and (f) the adsorption energy as a function of the $d$-band centre. $i$ stands for the $i$th layer ($i = 1,2$). Solid vertical line through (a), (b) and (c) denotes the Fermi level ($E_F$), grey dotted vertical lines denote the $d$-band centre in the valence band, and horizontal dotted lines in (d) and (e) denote the bulk value. The dashed line in (f) is a guide to the eye.